JOM, Vol. 64, No. 1, 2012
DOI: 10.1007/s11837-011-0223-y

Application of Neutron Scattering in Earth Sciences

H.-R. WENK[1,2]

1.—Department of Earth and Planetary Science, University of California, Berkeley, CA 94720, USA. 2.—e-mail: wenk@berkeley.edu

The unique properties of neutron interaction with materials have long been applied to the study of geological materials, with Shull and Smart using them in 1949 to determine the antiferromagnetic structure of manganosite (MnO). Neutron diffraction provides an accurate method for crystal structure determination of hydrous phases, particularly ices, and investigations of cation ordering of elements that are adjacent in the Periodic Table, such as Al–Si in feldspars and zeolites. Both elastic and inelastic scattering have been used to determine the properties of fluids that are present in many sedimentary rocks, including shales that are often saturated with brines or hydrocarbons. Due to minimal absorption and deep sample penetration, neutron scattering has become a favorite tool for crystallographic preferred orientation (texture) analysis of rocks as well as destruction-free three-dimensional (3D) tomographic characterization of microstructures.

INTRODUCTION

For over half a century neutron scattering has been used to determine the crystal structure of minerals, for instance, the alignment of magnetic spins in manganosite MnO,[1] and some early applications of neutron texture analysis were on rocks.[2,3] Correspondingly, there is much literature on applications of neutron scattering for geological materials, which is summarized in two recent review volumes.[4,5] Here we highlight a few of the applications which make use of the unique properties of neutron scattering.

The reason for using neutrons for the characterization of geological materials is the fundamental difference in scattering properties of x-rays and neutrons. While x-rays scatter on electrons, and thus scattering factors are directly related to atomic number, neutrons scatter on atomic nuclei and scattering factors vary in a nonsystematic way, depending on nuclear forces in isotopes. Neutron scattering factors can be positive or negative; for example, hydrogen has a negative scattering length (−3.74 fm, 1 femtometer = 10^{-15} m = 1 Fermi), whereas deuterium has a positive scattering length (6.67 fm), which is almost as strong as that of gold (7.63 fm). In comparison, the x-ray scattering factor of hydrogen is 1 and that of gold 79, making hydrogen practically invisible in the presence of heavier atoms. Hence for hydrous phases, including many minerals such as ice, hydroxides, phyllosilicates, and zeolites, neutron scattering is the ideal method to determine the crystallographic position of hydrogen. Also, adjacent elements in the Periodic Table have very similar x-ray scattering factors but can vary greatly for neutrons (Table I); for example, the neutron scattering length of Mn (Z = 25) is −3.73 fm and for Fe (Z = 26) it is 9.54 fm. Neutron diffraction is a favorite method to investigate ordering in such minerals. Neutrons have a magnetic spin and interact with magnetic spins of atoms in the crystal structure and have also been used to determine the magnetic structure of minerals such as manganosite, magnetite, and hematite.

Until 1980, the main geoscience application of neutron scattering was for crystal structure determination, mainly for single crystals, with monochromatic neutrons provided at reactor sources. With advances in powder diffraction, combined with the Rietveld refinement method,[6] crystal structure, microstructural parameters, as well as stress and strain can be refined simultaneously. Powder diffraction was further advanced by using pulsed neutrons and time-of-flight (TOF) detection, efficiently recording full diffraction spectra simultaneously. Many neutron facilities have environmental equipment that allows correlations of structural changes with temperature and pressure to establish phase diagrams.

(Published online February 11, 2012)

Table I. Atomic number (Z), coherent (b_{coh}) and incoherent nuclear scattering amplitudes (b_{inc}), magnetic scattering amplitude at $\Theta = 0$ (p) (all in fm = 10^{-15} m = 1 Fermi), as well as absorption cross-section σ for 2.2 km s^{-1} neutrons (in barns = 10^{-28} m^2 = 100 fm^2) for some geologically important elements

Atom/Ion	Z	b_{coh}	b_{inc}	p	σ
^{1}H	1	−3.74	25.2		33
D = ^{2}H	1	6.67	4.03		0
^{6}Li	6	2.00	−1.89		94000
^{7}Li	6	−2.22	−2.49		5
C	6	6.65	0		0
O	8	5.80	0		0
Mg	12	5.38	0		6
Al	13	3.45	0.26		23
Si	14	4.15	0		17
^{35}Cl	17	11.7	6.1		4410
^{37}Cl	17	3.1	0.1		43
Ca	20	4.70	0		43
Mn^{2+}	25	−3.73	1.79	13.5	1330
Fe^{2+}	26	9.54	0	10.8	256
Au	79	7.63	−1.84		9865
Pb	82	9.40	0		17

If isotope is not indicated, values are for natural abundance. For more information go to http://www.ncnr.nist.gov/resources/n-lengths/

Herein, some examples referring to detailed crystal structure analysis, characterization of disordered materials and bonding, quantification of microstructural features, characterization of preferred orientation, and destruction-free tomography are discussed. It must be emphasized that neutrons are no substitute for x-rays and much information is obtained by combining both methods, making use of their complementary properties.

Crystal Structure Analysis

Atomic positions in a periodic crystal structure are determined by analyzing elastic diffraction intensities. This technique provides information about the location, identity, thermal vibrations, and magnetic spin orientations of atoms. Either single crystals or powders may be used; however, because they are easier to prepare, powders are increasingly applied. X-rays scatter on electrons distributed over the large electron shell, whereas neutrons scatter on the tiny nucleus. The advantage for neutrons is that atomic positions are well defined and diffraction intensities (scattering factors) do not decrease with diffraction angle; they have the disadvantage that only few neutrons interact with atoms, and thus diffraction intensities are very weak, calling for large sample volumes of the order of cm^3. Often large single crystals are not available. Powerful computer programs have been developed in order to refine crystal structures based on relative intensities in the powder diffraction spectrum using the Rietveld method,[6] for example, FULLPROF,[7] GSAS,[8] and MAUD.[9]

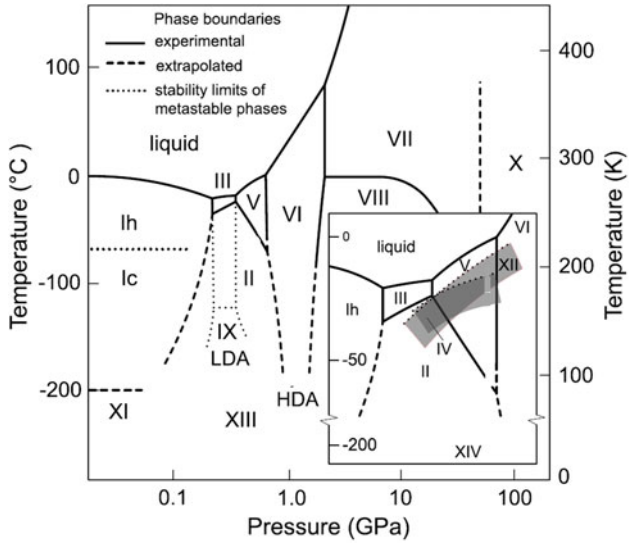

Fig. 1. Phase diagram of water and water ices including some recently discovered stable and metastable forms. The inset shows an enlarged part of the medium pressure range where several forms of ice coexist.[11,12]

Hydrogen

As mentioned above, hydrogen, with only one electron, is practically invisible to x-rays. On the other hand, both hydrogen (H) and deuterium (D) have neutron scattering factors that are comparable to heavy elements. The very complex pressure–temperature phase diagram of water (H_2O–D_2O) (Fig. 1) could never have been established without neutron diffraction.[10–12] It includes stable and metastable phases, many crystalline, but some amorphous. With hydrogen being the most common element in the Universe, ice is a common component on Earth and on the outer planets; thus its structure is critical for understanding planetary evolution. Especially fascinating is the discovery of low- and high-density amorphous ice compounds.[13,14]

Recently gas hydrates have received much attention, both as hydrocarbon reservoirs at continental shelves as well as for hydrogen and carbon dioxide (CO_2) storage. The complex structures of clathrates, especially methane and CO_2 clathrates with large asymmetric cages, have been refined from neutron scattering data.[15–17] *In situ* experiments quantified the decomposition of metastable gas hydrates as a function of temperature and time[18] (Fig. 2).

Water is present in many minerals, such as the hydroxides boehmite $Fe(OH)_2$[19,20] and brucite $Mg(OH)_2$. For trigonal brucite, hydrogen is largely disordered at ambient conditions (Fig. 3a), but distinctly ordered at high pressure[21] (Fig. 3b). Water in gypsum $CaSO_4(OH)_2$,[22] ikaite $CaCO_3(H_2O)_6$,[23,24] and hydroxylapatite $Ca_5OH(PO_4)_3$[25] was investigated by neutron diffraction. Much attention has

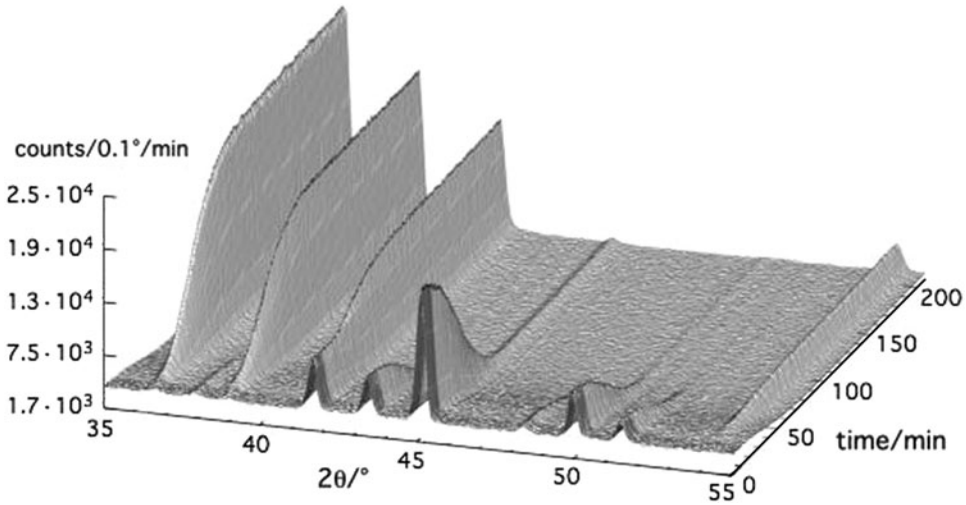

Fig. 2. Decomposition of CO_2 gas hydrates with decreasing pressure at 210 K. Diffraction spectra were recorded with the position-sensitive detector D20 at ILL.[18]

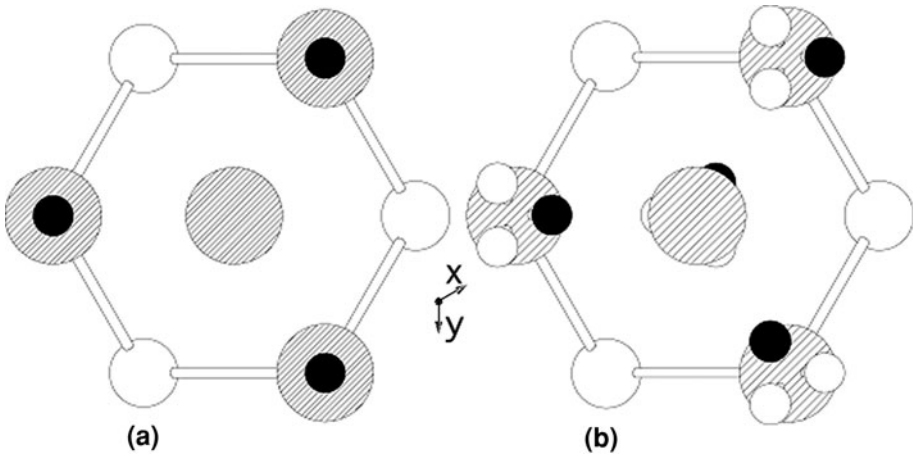

Fig. 3. Structure of deuterated brucite $Mg(OD)_2$ projected along [0001]. Striped circles are oxygen, large white circles are magnesium, and small black and white circles are deuterium. At ambient conditions D occupies a single site (a), but at high pressure (>10 GPa) D splits into three equivalent sites. Small black circles represent one possible model for the occupancy of the deuterium sites. Based on *in situ* powder diffraction measurements with HIPD at LANSCE.[21]

been dedicated to zeolites, silicates with open cage structures such as natrolite $Na_2[Al_2Si_3O_{10}]\cdot 2H_2O$,[26] gismondine $Ca[Al_2Si_2O_8]\cdot 4H_2O$,[27] and yugawaralite $Ca[Al_2Si_5O_{14}]\cdot 3H_2O$.[28,29] Besides natural zeolites, the structure of benzene[30] and xylene molecules[31] in the technologically important zeolite Y, applied for petroleum refinement, helped identify catalytically active sites.

Ordering

Many minerals form solid solutions between end-member compositions, and the determination of the ordering pattern is critical for establishing thermodynamic stability. Examples are Al–Si in feldspars and zeolites and Fe–Mn in olivine, spinel, and perovskite. Both Al–Si and Mn–Fe are adjacent pairs of elements in the Periodic Table and hardly distinguishable by x-rays (Table I). Neutron diffraction can establish the Al–Si ordering pattern in the feldspar albite,[32] and in the zeolite natrolite, which is fully ordered at high pressure,[26,33] whereas synthetic sodalite $Na_8[Cl_2|(AlSiO_4)_6]$ is disordered at high temperature[34] but ordered at lower temperature.[35]

Fe–Mn ordering has been studied in the fayalite Fe_2SiO_4-tephroite Mn_2SiO_4 solid solution with olivine structure,[36–38] and magnetite Fe_3O_4-hausmannite Mn_3O_4 with spinel structure, including jacobsite $MnFe_2O_4$.[39,40]

Magnetic Structure

Magnetic scattering is due to dipole–dipole interaction between the magnetic moments of neutrons and that of atoms. It is of similar magnitude to the nuclear scattering (Table I).[41] The classic first application was to look into the magnetic structure

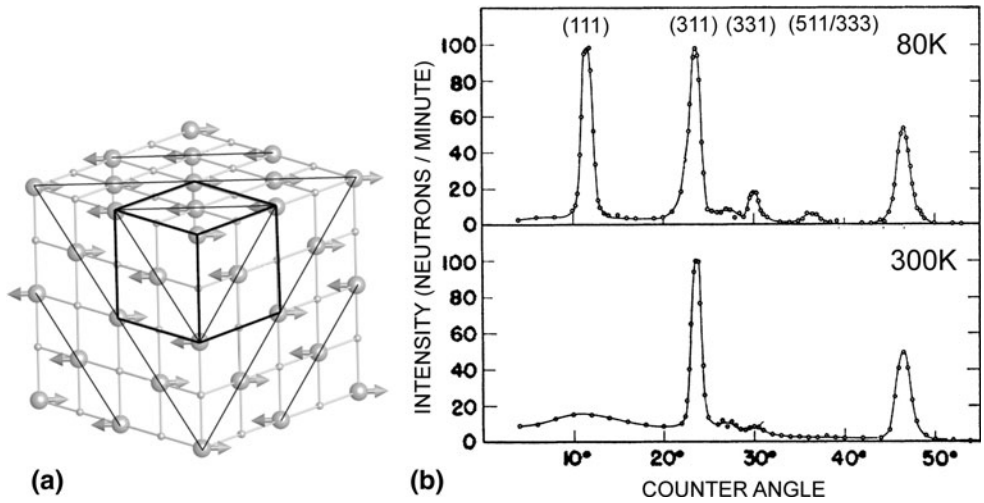

Fig. 4. Magnetic structure of manganosite MnO. (a) Structure with O (small open spheres) and Mn (arrowed large spheres), arrows showing magnetic dipole orientation. Note the opposite alignment in adjacent (111) planes. The crystallographic cubic unit cell is indicated by heavy black lines. The magnetic unit cell covers the whole picture. (b) Neutron diffraction spectra of MnO below (top) and above (bottom) the Néel temperature. Peaks such as 111 and 331 are only due to magnetic ordering.[1]

of manganosite MnO, which has a cubic NaCl structure. Shull and Smart determined in 1949 the magnetic structure and found that spins are aligned parallel to <110> and adjacent dipoles point in opposite directions (Fig 4a).[1] The magnetic structure, as displayed by dipoles, no longer has cubic symmetry, and furthermore the unit cell is doubled along all axes owing to the alternating magnetic dipoles. The results reveal that, in this ferrimagnetic mineral, additional reflections such as 111 and 331 appear in the neutron diffraction pattern at low temperature (80 K), but not in x-ray diffraction patterns or the neutron diffraction pattern taken above the Néel temperature (116 K) where spins become disordered (Fig. 4b). Because dipole directions cancel, there is no bulk macroscopic magnetic behavior, making neutron diffraction the only method to detect the magnetic order.

The situation is more complex in magnetite Fe_3O_4 with spinel structure. Here dipoles do not cancel, and there is a remaining ferromagnetic behavior.[42] Magnetism of magnetite has been studied not only in large crystals but also in fine-grained magnetotactic bacteria.[43]

In rhombohedral hematite Fe_2O_3, below the Morin temperature,[44,45] all spins are parallel to [0001] in (0001) layers, though alternating in direction in adjacent layers (Fig. 5a). This is different in the isostructural mineral eskolaite Cr_2O_3 where dipoles in a layer alternate[46] (Fig. 5b). The dipole alignment in hematite varies as a function of temperature and pressure.[47]

Thermal Vibration

As mentioned earlier, neutron scattering factors do not attenuate with diffraction angle (i.e., inverse *d*-spacing). If attenuation is observed, it is solely due to thermal vibrations and can be used to quantify anisotropic temperature factors and static disorder. Such data established OH^- motions with temperature in chondrodite,[48] loss of 3D long-range order in ferroelastic Na_2CO_3,[49] elliptical distortions of F in $KCaF_3$ perovskite,[50] and rotational disorder of oxygen in calcite at high temperature as illustrated in Fourier maps[51] (Fig. 6). *In situ* studies investigated the role of thermal motion of deuterium atoms on the decomposition of portlandite $Ca(OH)_2$, an important mineral in the cement industry.[52]

Since neutron diffraction provides accurate diffraction data for low *d*-spacings, it lends itself to determine charge density distributions, especially when combining x-rays and neutron scattering data.[53]

Disordered Materials

The discussion so far has emphasized elastic neutron scattering and diffraction. Inelastic neutron scattering, which involves energy and momentum exchange between neutrons and the scatterer, is another possibility. Energy transfer is particularly large for hydrogen and so provides information about vibrational modes associated with bonding. All vibrational modes occur at specific energies, depending on the bonding environment.

Inelastic scattering has been used to quantify the local bonding environment, not only of pure water, or water in rocks such as clays,[54–56] but also of geologic fluids containing molecules such as H_2O, CO_2, H_2, H_2S, N_2, and CH_4. A molecular-level understanding of the reactions and reactive interfaces between fluids and parent rock as a function of temperature and pressure provides a more predictive view of state-dependent reactions where neutron scattering adds crucial information and complements other techniques such as nuclear

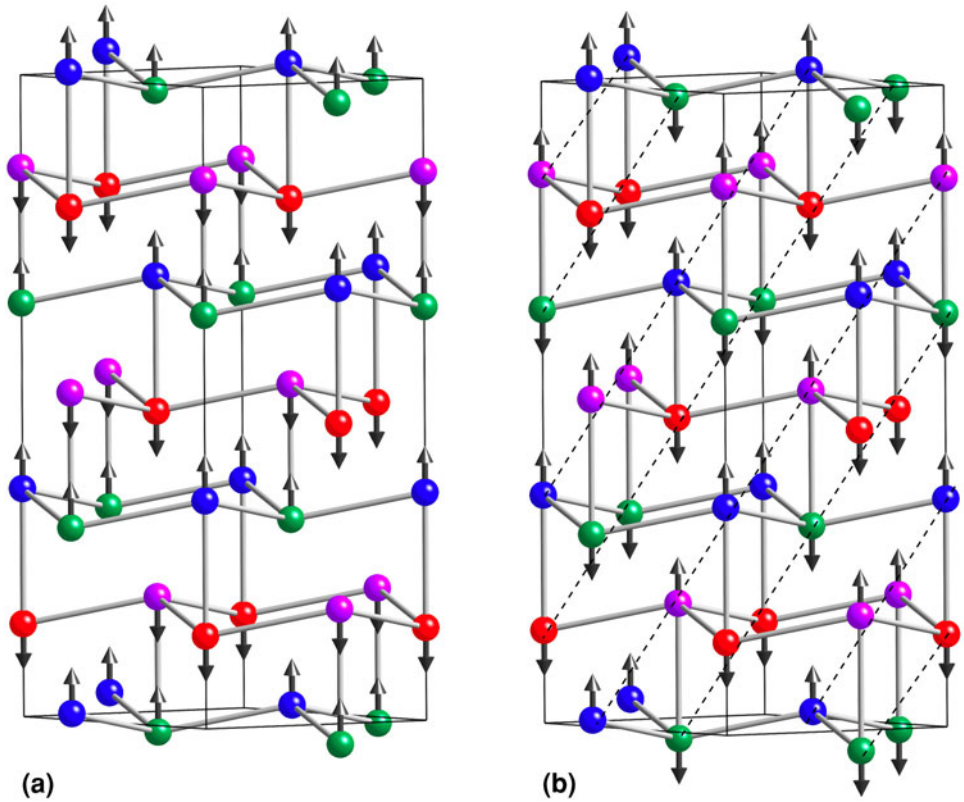

Fig. 5. Magnetic structure of (a) hematite Fe_2O_3 and (b) eskolaite Mn_2O_3. Only Fe and Mn atoms are shown, with arrows indicating magnetic dipoles. [0001] axis is vertical. Dashed lines illustrate ferromagnetically coupled layers.[45,46]

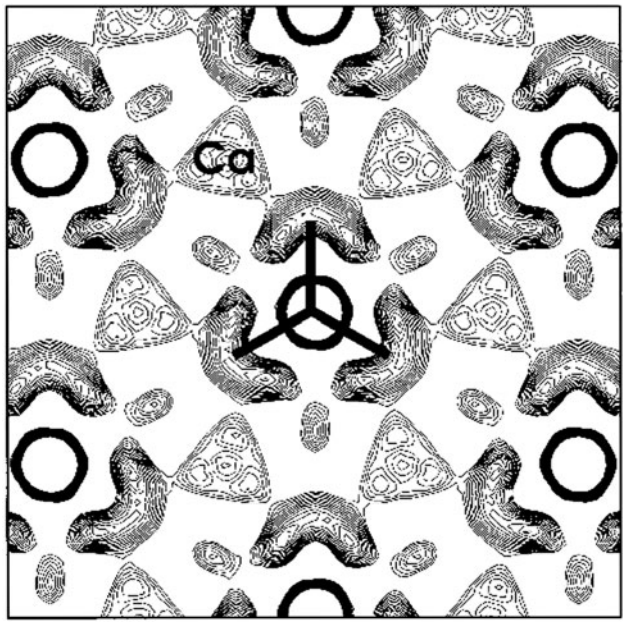

Fig. 6. Rotational disorder of oxygen at high temperature (1189 K) represented as a Fourier map. The open circles show the carbon positions; calcium (Ca) is indicated. The oxygen distributions at high temperature are banana shaped around [0001], producing hexagonal symmetry. Analysis based on powder spectra collected with DUALSPEC at Chalk River.[51]

magnetic resonance (NMR) and infrared (IR) spectroscopy.[57]

In addition to neutron diffraction, inelastic neutron spectroscopy has been critical in understanding the phase diagram of water (Fig. 1); For example, comparison of neutron vibrational spectra with hydrogen and deuterium-exchanged water contribute to a better understanding of hydrogen bonding.[58–60] With neutron diffraction with isotopic substitution (NDIS) for ^{35}Cl–^{37}Cl, the arrangement of water molecules around cations within saline solutions was characterized.[61] Crystal field splitting was documented in xenotime $YbPO_4$, both at ambient conditions and as a function of temperature.[62] In hydroxylapatite it was observed that stretching vibrations of 011 modes only exist in synthetic powders but not in natural bones.[63]

Disordered materials, including amorphous compounds and liquids with only short-range order, have been analyzed with small-angle neutron scattering (SANS). Important applications are amorphous ice with tetrahedral networks resembling liquid water.[59,64] Local order can be established with the pair distribution function (PDF) which describes the closest neighbor environment of atoms.[65] Figure 7 shows the difference of a SANS PDF spectrum of amorphous silica glass and crystalline quartz SiO_2.[66] The first peaks are very sim-

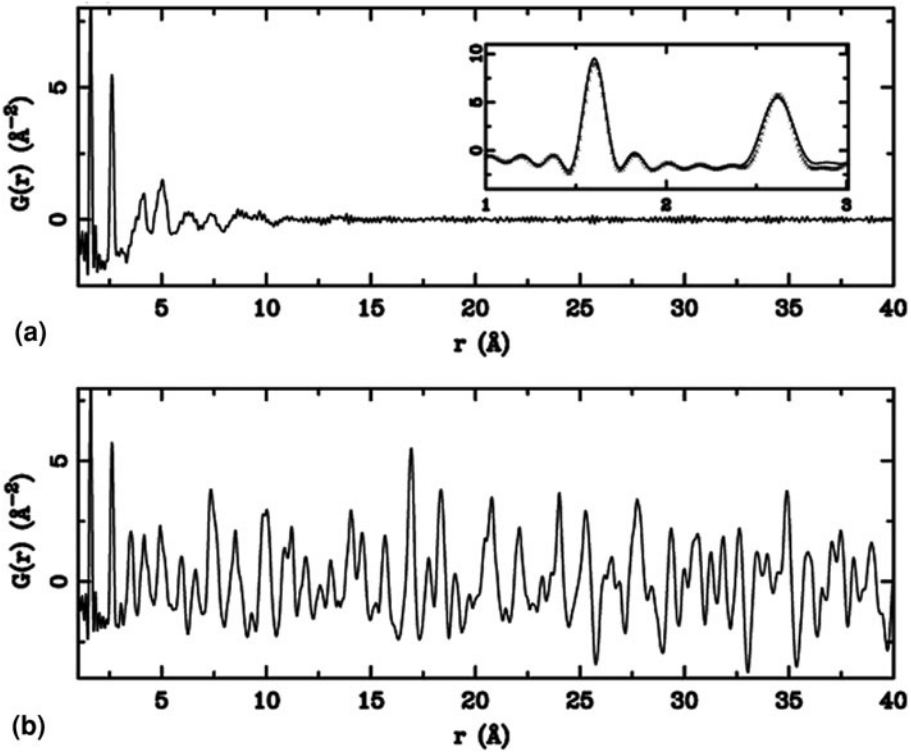

Fig. 7. Pair distribution function of (a) SiO_2 glass and (b) crystalline quartz measured with the small-angle scattering diffractometer NPDF at LANSCE. The low-distance part of spectrum (a) is enlarged as inset and shows the two first peaks attributed to Si–O (1.6) and O–O (2.6) tetrahedral spacings.[66]

ilar and correspond to tetrahedral Si–O distances (1.6 Å) and O–O distances (2.6 Å), but there is no higher-order structure in the amorphous phase. SANS has been used to describe the microstructure of the amorphous hydrous SiO_2 polymorph opal and establish not only nearest-neighbor geometries but also size of spherulitic SiO_2 particles.[67]

An important application of SANS has been to establish the microstructure of porous sandstones which are source rocks for hydrocarbons. Figure 8a displays pore size distribution and specific surface area calculated from SANS spectra as a function of size.[68] The calculated pore volume based on SANS measurements is in excellent agreement with values obtained directly by mercury injection porosimetry (Fig. 8b). SANS has been used to study *in situ* migration of fluids in porous rocks as well as cements.[69–71]

Texture and Strain

While much of the previous discussion has focused on the unique scattering characteristics of neutrons—particularly the strong interaction of neutrons with hydrogen and deuterium—we now illustrate applications that make use of the very high sample penetration that allows one to analyze large volumes *in situ*. This is particularly significant to investigate residual stresses and determine preferred orientation in coarse-grained rocks. We will first discuss texture analysis and then show a few examples of strain analysis.

For most elements, attenuation (i.e., reduction of incident intensity by scattering and absorption) for neutrons is an order of magnitude weaker than for x-rays. This results in penetration depths of the order of cm for neutrons instead of mm as is the case for x-rays, or μm for electrons. Large samples (1 cm to 10 cm in diameter) of roughly spherical shape can be measured. Because the diffraction signal averages over large volumes rather than surfaces, grain statistics are better than with conventional x-rays. Figure 9 illustrates statistical limitations for an experimentally deformed calcite marble. Pole figures were measured with an x-ray pole figure goniometer in reflection geometry on the surface of a slab (Fig. 9a) and by neutron diffraction on a 1-cm^3 sample cube (Fig. 9b).[3] The x-ray pole figure shows an irregular pattern, whereas the neutron pole figure displays a symmetrical distribution, representative of the bulk deformation geometry. The low absorption has other advantages: Intensity corrections are generally unnecessary, and environmental stages (heating, cooling, straining) can be used for *in situ* observation of texture changes.

Neutron diffraction texture studies are performed either at reactors with a constant flux of thermal neutrons, or with pulsed neutrons at spallation sources. Both techniques have produced very reliable results, as was tested by circulating a textured

polycrystalline calcite sample among 15 different neutron diffraction facilities.[9,72–75] Four examples are shown in Fig. 10. For pole figures with strong diffraction intensities, standard deviations from the mean are 0.04 to 0.06 multiples of random distribution (m.r.d.). For weak diffraction peaks, position-sensitive detectors and TOF techniques have an advantage over single tube detectors with monochromatic neutrons, since integrated rather than peak intensities are determined, which yield better counting statistics.

For TOF experiments, where full diffraction spectra are recorded simultaneously, the Rietveld method provides the most efficient analysis of textures.[9,74,76] By analyzing the whole spectrum, individual diffraction peaks do not have to be separated, which is particularly beneficial for low-symmetry compounds and composites with many overlapping peaks. Figure 11 shows an example of gneiss composed of quartz, feldspar, and biotite mica.[77] Individual diffraction peaks are indicated underneath the intensity profile. The Rietveld analysis not only provides texture information for individual phases (here represented as individual pole figures) but also volume fractions and crystallographic information. Instruments widely used for neutron texture analysis are HIPPO at LANSCE, with count times of the order of 1 h for most geological samples and the ability to measure texture at temperatures up to 1300 K, and SKAT at JINR.

While neutron scattering is increasingly used to determine residual stress in deformed metals,[78–80] there have been only few applications for geological materials. This is because lattice strains are generally small, especially when averaged over a large polycrystalline sample, and are beyond the resolution of instruments such as ENGIN-X at ISIS, EPSILON at JINR, or SMARTS at LANSCE. Nevertheless, some interesting results have been obtained, e.g., for elastic strain partitioning in polyphase rocks.[81,82] By straining rocks *in situ*, mechanical twinning can be induced, as was documented for calcite[83] and quartz.[84]

Besides applying stress via a load frame, the stresses imposed by thermal expansion during heating of an aggregate play important roles in the mechanical stability of mineral or cement aggregates, and

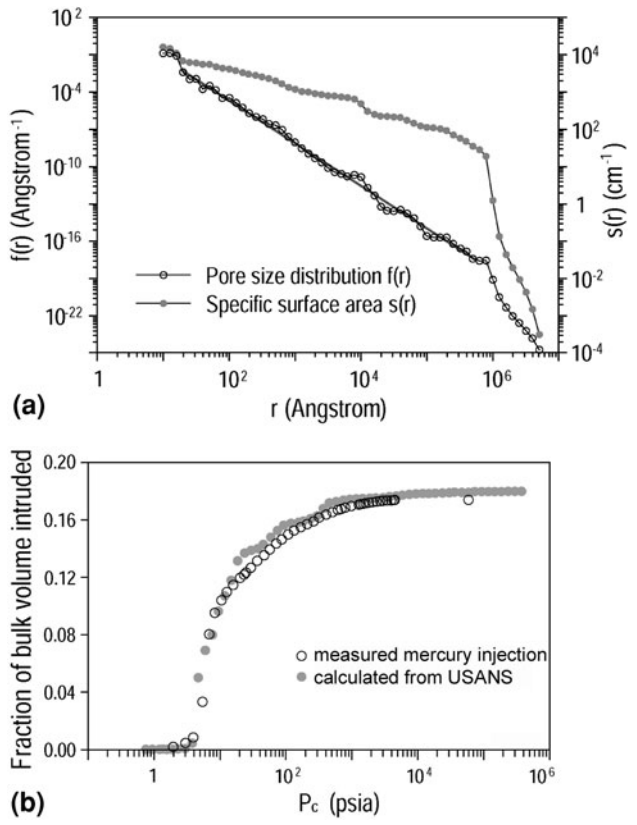

Fig. 8. Microstructure of sandstone investigated with USANS diffractometer at ORNL. (a) Distribution of pore size [$f(r)$] and specific surface area [$s(r)$]. (b) Fraction of bulk pore volume calculated from USANS experiments and compared with mercury intrusion porosimetry.[68]

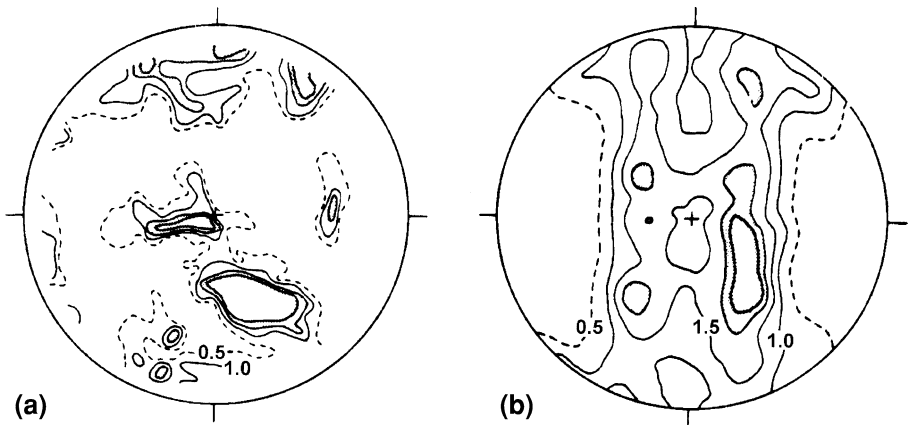

Fig. 9. Comparison of (0006) pole figures of calcite for experimentally deformed marble: (a) measured by x-ray diffraction in reflection geometry, and (b) measured by monochromatic neutron radiation in Jülich. Equal-area projection, contours in multiples of a random distribution.[3]

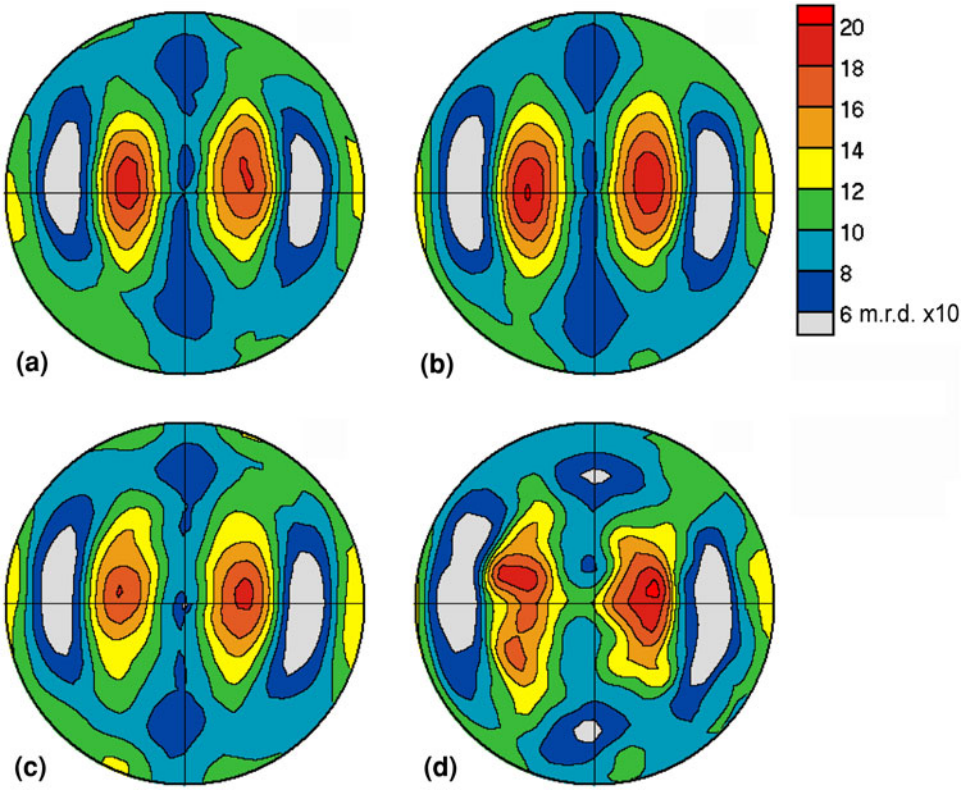

Fig. 10. Calcite 0001 pole figures of an experimentally deformed limestone standard sample, used in a round-robin to assess reliability of neutron diffraction texture measurements. Examples are from measurements at four neutron diffraction facilities: (a) conventional reactor with monochromatic neutrons (Julios at KFA, Jülich[72]), (b) reactor with monochromatic neutrons and position-sensitive detector (D1B at ILL, Grenoble[72]), (c) pulsed reactor with TOF measurements, single peak extraction (SKAT at Dubna, Russia[73]), (d) spallation neutrons with 30 detectors and texture determined with the Rietveld method (HIPPO at LANSCE, Los Alamos[75]). Equal-area projection, linear contours.

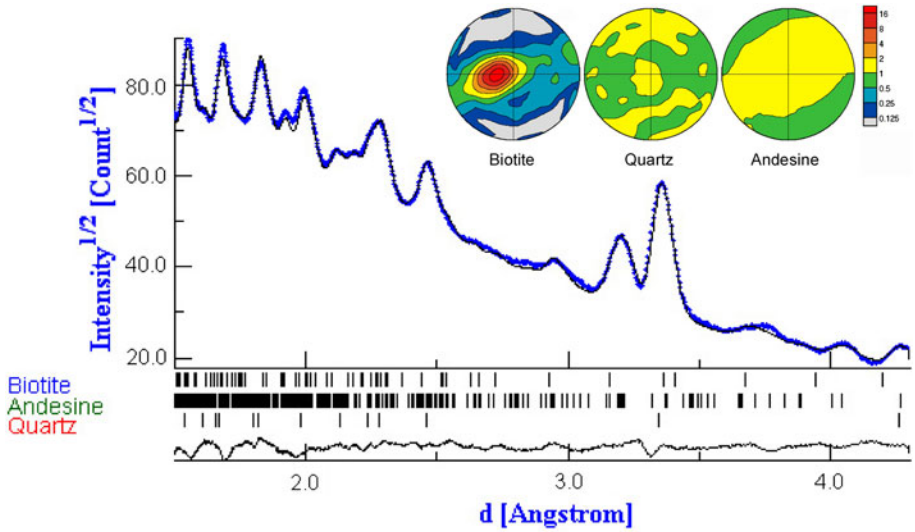

Fig. 11. Texture analysis of gneiss composed of quartz, feldspar (andesine), and mica (biotite) with the Rietveld method implemented in MAUD. Spectra were measured with the TOF diffractometer HIPPO at LANSCE, and data for one 90° detector are shown. Blue is the measured diffraction intensity, and the black line is the Rietveld fit. Below, diffraction lines of the phases are indicated. (001) pole figures of the phases are shown as insets (Color figure online).[77]

neutrons have proven themselves to be a valuable tool to measure the anisotropy, i.e., the lattice direction-dependent thermal expansion, of, e.g., gypsum $CaSO_4{\cdot}2H_2O$,[85] portlandite $Ca(OD)_2$,[52,86] cordierite $(Mg,Fe)_2Al_3(Si_5AlO_{18})$,[87,88] or jarosite $KFe_3(SO_4)_2(OD)_6$.[89]

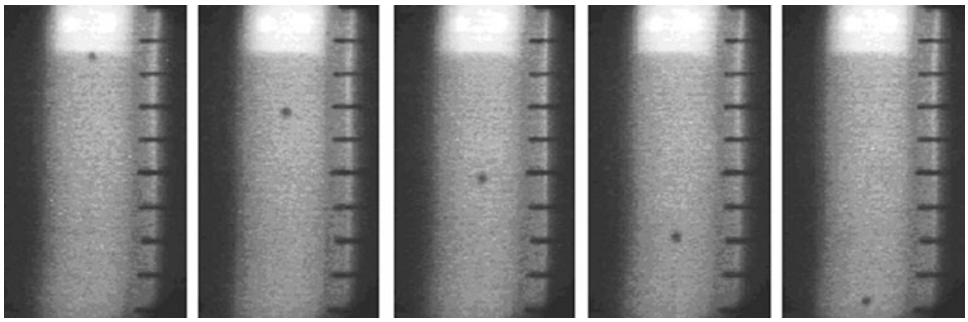

Fig. 12. Time-dependent neutron radiography. A sphere made of strongly absorbing material (Hf) falls in a silicate melt at high temperatures (>1000°C). From the speed, the viscosity of the melt can be determined. The distance between the markers on the right of each frame is 1 cm.[93]

Tomography

Because of the high penetration of neutrons for most materials, destruction-free characterization of large geological objects by 3D microtomography is possible. The sample is viewed in different directions, and images are processed to provide a 3D representation of absorption characteristics. Liquid-filled pores and dynamic investigations of liquid flow through porous materials are of great interest.[90–92] Neutron tomography has also been used to study viscosity of silicate melts by observing velocities of a falling sphere[93] (Fig. 12). By using different energies, specific components can be highlighted.[94] Introducing high-resolution detectors, neutron tomography can currently resolve 20 μm.[95,96] Although the resolution of neutron tomography is still limited compared with x-ray microtomography at synchrotron sources, much larger samples can be analyzed. A review of geological applications of neutron tomography is available.[97]

CONCLUSIONS

Neutron scattering has been of critical importance in the characterization of earth materials. The magnetic structure of minerals and crystal structures of hydrous phases could not have been achieved without neutrons. The best example is the complex phase diagram of water. Earth scientists are becoming increasingly engaged in neutron experiments on rocks, for example, to study *in situ* the internal microstructure by 3D tomography, to investigate fluid phases in shales, and to quantify preferred orientation. For earth sciences, reaching high pressures comparable to the deep Earth has been critical. So far neutrons have been limited for such applications, but this may change in the future. Highly focused neutron beams of the order of 10 micrometers can be produced, being comparable to synchrotron x-rays,[98] and with moissanite anvil cells, pressures of 65 GPa have been reached on samples >2 mm^3.[99]

ACKNOWLEDGEMENTS

The author acknowledges support from NSF and DOE. He is appreciative for access to neutron facilities at ILL, IPNS, ISIS, and especially LANSCE. This paper is dedicated to Alan Hurd, who has succeeded in developing the Lujan Center at Los Alamos into a prestigious neutron user facility. The author is appreciative for comments on the manuscript by John Carpenter, Waruntorn Kanitpanyacharoen, Pamela Kaercher, Sven Vogel, and Eloisa Zepeda.

REFERENCES

1. C.G. Shull and J.S. Smart, *Phys. Rev.* 76, 1256 (1949).
2. H.-J. Bunge, H.-R. Wenk, and J. Pannetier, *Textures Microstruct.* 5, 153 (1982).
3. H.-R. Wenk, H. Kern, W. Schäfer, and G. Will, *J. Struct. Geol.* 6, 687 (1984).
4. L. Liang, R. Rinaldi, and H. Schober, eds., *Neutron Applications in Earth, Energy and Environmental Sciences* (New York: Springer, 2009).
5. H.-R. Wenk, ed., *Neutron Scattering in Earth Sciences*. Reviews in Mineralogy and Geochemistry, vol. 63 (Chantilly, VA: Mineralogical Society of America, 2006).
6. H.M. Rietveld, *J. Appl. Crystallogr.* 2, 65 (1969).
7. J. Rodriguez-Carvajal, *FULLPROF: A Program for Rietveld Refinement and Pattern Matching Analysis* (1990), www.llb.cea.fr/fullweb/fp2k/fp2k.htm.
8. A.C. Larson and R.B. Von Dreele, General Structure Analysis System (GSAS). Los Alamos National Laboratory Report LAUR 86-748 (2004).
9. L. Lutterotti, S. Matthies, H.-R. Wenk, A.J. Schultz, and J.W. Richardson, *J. Appl. Phys.* 81, 594 (1997).
10. W.F. Kuhs, J.L. Finney, C. Vettier, and D.V. Bliss, *J. Chem. Phys.* 81, 3612 (1984).
11. C. Lobban, J.L. Finney, and W.F. Kuhs, *J. Phys. Chem.* 112, 7169 (2000).
12. C.G. Salzmann, P.G. Radaelli, A. Hallbrucker, E. Mayer, and J.L. Finney, *Science* 311, 1758 (2006).
13. O. Mishima and H.E. Stanley, *Nature* 396, 329 (1998).
14. T. Loerting, W. Schustereder, K. Winkel, C.G. Salzmann, I. Kohl, and E. Mayer, *Phys. Rev. Lett.* 96, 025702 (2006).
15. R.W. Henning, A.J. Schultz, V. Thien, and Y. Halpern, *J. Phys. Chem.* 104, 5066 (2000).
16. X. Wang, A.J. Schultz, and Y. Halpern, *J. Phys. Chem. A* 106, 7304 (2002).
17. W.F. Kuhs, D.K. Staykova, and A.N. Salamatin, *J. Phys. Chem. B* 110, 13283 (2006).
18. W.F. Kuhs, G. Genov, D.K. Staykova, and T.C. Hansen, *Phys. Chem. Chem. Phys.* 6, 4917 (2004).

19. A. Szytula, A. Burewicz, Z. Dimitrijevic, S. Krasnicki, H. Rzany, J. Todorovic, A. Wanic, and W. Wolski, *Phys. Status Solidi* 26, 429 (1968).
20. A.N. Christensen, M.S. Lehmann, and P. Convert, *Acta Chem. Scand. Ser. A* 36, 303 (1982).
21. J.B. Parise, K. Leinenweber, D.J.K.T. Weidner, and R.B. Von Dreele, *Am. Mineral.* 79, 193 (1994).
22. P.F. Schofield, K.S. Knight, and I.C. Stretton, *Am. Mineral.* 81, 847 (1996).
23. K.F. Hesse, H. Küppers, and E. Suess, *Z. Kristallogr.* 163, 227 (1970).
24. I.P. Swainson and R.P. Hammond, *Mineral. Mag.* 67, 555 (2003).
25. T. Leventouri, B.C. Chakoumakos, N. Papanearchou, and B. Perdikatsis, *J. Mater. Res.* 16, 2600 (2001).
26. G. Artioli, J.V. Smith, and Å. Kvick, *Acta Crystallogr.* C40, 1658 (1984).
27. G. Artioli, R. Rinaldi, Å. Kvick, and J.V. Smith, *Zeolites* 6, 361 (1986).
28. Å. Kvick, G. Artioli, and J.V. Smith, *Zeit. Krist.* 174, 265 (1986).
29. G. Artioli, K. Ståhl, G. Cruciani, A. Gualtieri, and J.C. Hanson, *Am. Mineral.* 86, 185 (2001).
30. A.N. Fitch, H. Jobic, and A. Renouprez, *J. Phys. Chem.* 90, 1311 (1986).
31. M. Czjzek, H. Fuess, and T. Vogt, *J. Phys. Chem.* 95, 5255 (1991).
32. J.V. Smith, G. Artioli, and Å. Kvick, *Am. Mineral.* 71, 727 (1986).
33. M. Colligan, Y. Lee, T. Vogt, A.J. Celestian, J.B. Parise, W.G. Marshall, and J.A. Hriljac, *J. Phys. Chem. B* 109, 18223 (2005).
34. S.E. Tarling, P. Barnes, and J. Klinowski, *Acta Crystallogr. B* 44, 128 (1988).
35. R.K. McMullan, S. Ghose, N. Haga, and V. Schomaker, *Acta Crystallogr.* B52, 616 (1996).
36. C.M.B. Henderson, K.S. Knight, S.A.T. Redfern, and B.J. Wood, *Science* 271, 1713 (1996).
37. S.A.T. Redfern, C.M.B. Henderson, K.S. Knight, and B.J. Wood, *Eur. J. Mineral.* 9, 287 (1997).
38. S.A.T. Redfern, K.S. Knight, C.M.B. Henderson, and B.J. Wood, *Mineral. Mag.* 62, 607 (1998).
39. U. Koenig and G. Chol, *J. Appl. Crystallogr.* 1, 124 (1968).
40. V. Baron, J. Gutzmer, H. Rundloef, and R. Tellgren, *Am. Mineral.* 83, 786 (1998).
41. P.J. Brown, *International Tables for Crystallography*, Volume C, ed. A.J.C. Wilson (Dordrecht: Kluwer, 1995), p. 391.
42. C.G. Shull, E.O. Wollan, and W.C. Koehler, *Phys. Rev.* 84, 912 (1951).
43. S. Krueger, G.J. Olson, J.J. Rhyne, R.P. Blakemorre, Y.A. Gorby, and N. Blakemore, *J. Appl. Phys.* 67, 4475 (1990).
44. C.G. Shull, W.A. Strauser, and E.O. Wollan, *Phys. Rev.* 83, 333 (1951).
45. R.J. Harrison, S.A.T. Redfern, and R.I. Smith, *Am. Mineral.* 85, 194 (2000).
46. A.S. Wills, *Phys. Rev. B* 63, 064430 (2001).
47. J.B. Parise, D.R. Locke, C.A. Tulk, I. Swainson, and L. Cranswick, *Physica B* 385, 391 (2006).
48. M. Kunz, G. Lager, H.B. Burgi, and M.T. Fernandez-Diaz, *Phys. Chem. Miner.* 33, 17 (2006).
49. M.J. Harris, M.T. Dove, and K.W. Godfrey, *J. Phys. Condens. Matter* 8, 7073 (1996).
50. D.Z. Demetriou, C.R.A. Catlow, A. Chadwick, G.J. McIntyre, and I. Abrahams, *Solid State Ionics* 176, 1571 (2005).
51. M.T. Dove, I.P. Swainson, B.M. Powell, and D.C. Tennant, *Phys. Chem. Miner.* 32, 493 (2005).
52. H. Xu, Y. Zhao, S.C. Vogel, L.L. Daemen, and D.D. Hickmott, *J. Solid State Chem.* 180, 1519 (2007).
53. G. Artioli, *Eur. J. Mineral.* 14, 233 (2002).
54. G. Sposito, N.T. Skipper, R. Sutton, S.H. Park, A.K. Soper, and J.A. Greathouse, *Proc. Nat. Acad. Sci. USA* 96, 3358 (1999).
55. N.T. Skipper, G.D. Williams, A.V.C. de Siqueira, C. Lobban, and A.K. Soper, *Clay Miner.* 35, 283 (2000).
56. N. Malikova, A. Gadéne, V. Marry, E. Dubois, P. Turq, J.-M. Zanotti, and S. Longeville, *Chem. Phys.* 317, 226 (2005).
57. D.R. Cole, M.S. Gruszkiewicz, J.M. Simonson, A.A. Chialvo, Y.B. Melnichenko, G.D. Wignall, D.R. Cole, and H. Frielinghaus, *Water–Rock Interaction*, vol. 1, ed. R. Want and R. Seal (Saratoga Springs, New York, 2004), pp. 735–739.
58. B. Bruni, M.A. Ricci, and A.K. Soper, *Phys. Rev. B* 54, 11876 (1996).
59. A.K. Soper, *Science* 297, 1288 (2002).
60. J. Dore, *J. Mol. Struct.* 250, 193 (1991).
61. J.E. Wilson, S. Ansell, J.E. Enderby, and G.W. Neilson, *Chem. Phys. Lett.* 278, 21 (1997).
62. C.-K. Loong, M. Loewenhaupt, J.C. Nipko, M. Braden, and L.A. Boatner, *Phys. Rev. B* 60, R12549 (1999).
63. C.-K. Loong, C. Rey, L.T. Kuhn, C. Combes, Y. Wu, S.-H. Chen, and M.J. Glimcher, *Bone* 26, 599 (2000).
64. J.L. Finney, D.T. Bowron, A.K. Soper, T. Loerting, E. Mayer, and A. Hallbrucker, *Phys. Rev. Lett.* 89, 205503 (2002).
65. T. Egami and S.J.L. Billinge, *Underneath the Bragg Peaks: Structural Analysis of Complex Materials*, 1st ed. (Amsterdam: Pergamon, 2003).
66. T. Proffen, *Neutron Scattering in Earth Sciences*. Reviews in Mineralogy and Geochemistry, vol. 63 (Chantilly, VA: Mineralogical Society of America, 2006), pp. 255–274.
67. H. Graetsch and K. Ibel, *Phys. Chem. Miner.* 24, 102 (1997).
68. A.P. Radlinski, M.A. Ioannidis, A.L. Hinde, M. Hainbuchner, M. Baron, H. Rauch, and S.R. Kline, *J. Colloid Interface Sci.* 274, 607 (2004).
69. A.J. Allen, *J. Appl. Crystallogr.* 24, 624 (1991).
70. A. Faraone, S.H. Chen, E. Fratini, P. Baglioni, L. Liu, C. Brown, *Phys. Rev. E* 65, 040501-1 (2002).
71. L. Jin, G. Rother, D.R. Cole, D.F.R. Mildner, C.J. Duffy, and S.L. Brantley, *Am. Mineral.* 96, 498 (2011).
72. H.-R. Wenk, *J. Appl. Crystallogr.* 24, 920 (1991).
73. K. Walther, K. Ullemeyer, J. Heinitz, M. Betzl, and H.-R. Wenk, *J. Appl. Crystallogr.* 28, 503 (1995).
74. R.B. Von Dreele, *J. Appl. Crystallogr.* 30, 517 (1997).
75. H.-R. Wenk, L. Lutterotti, and S. Vogel, *Nucl. Instrum. Methods A* 515, 575 (2003).
76. H.-R. Wenk, L. Lutterotti, and S.C. Vogel, *Powder Diffr.* 25, 283 (2010).
77. H.R. Wenk, H. Kern, S. Matthies, R. Vasin, and S. Vogel, *Tectonophysics* (submitted, 2012).
78. A.D. Krawitz, *Introduction to Diffraction in Materials Science and Engineering* (New York: Wiley, 2001).
79. M.T. Hutchings, P.J. Withers, T.M. Holden, and T. Lorentzen, *Introduction to the Characterization of Residual Stress by Neutron Diffraction* (Boca Raton: Taylor and Francis, 2005).
80. M.R. Daymond, *Neutron Scattering in Earth Sciences*. Reviews in Mineralogy and Geochemistry, vol. 63, Chapter 16, ed. H.-R. Wenk (Chantilly, VA: Mineralogical Society of America, 2006), pp. 427–434.
81. A. Frischbutter, D. Neov, C. Scheffzuk, M. Vrana, and K. Walther, *J. Struct. Geol.* 22, 1587 (2000).
82. S.J. Covey-Crump, P.F. Schofield, I.C. Stretton, K.S. Knight, and W.B. Ismail, *J. Geophys. Res. Solid Earth* 108(B2), 2092 (2003).
83. P.F. Schofield, S.J. Covey-Crump, I.C. Stretton, M.R. Daymond, K.S. Knight, and R.F. Holloway, *Mineral. Mag.* 67, 967 (2003).
84. H.-R. Wenk, M. Bortolotti, N. Barton, E. Oliver, and D. Brown, *Phys. Chem. Miner.* 34, 599 (2007).
85. K.S. Knight, I.C. Stretton, and P.F. Schofield, *Phys. Chem. Miner.* 26, 477 (1999).
86. E.M. Schulson, I.P. Swainson, and T.M. Holden, *Cem. Concr. Res.* 31, 1785 (2001).
87. G. Bruno and S. Vogel, *J. Am. Ceram. Soc.* 91, 2646 (2008).
88. G. Bruno, A.M. Efremov, B. Clausen, A.M. Balagurov, V.N. Simkin, B.R. Wheaton, J.E. Webb, and D.W. Brown, *Acta Mater.* 58, 1994 (2010).
89. H. Xu, Y. Zhao, S. Vogel, D.D. Hickmott, L.L. Daemen, and M.A. Hartl, *Phys. Chem. Miner.* 37, 83 (2009).
90. A. Nordlund, P. Linden, G. Por, M. Solymar, and B. Dahl, *Nucl. Instrum. Methods Phys. Res.* A462, 457 (2001).

91. F.C. de Beer, M.F. Middleton, and J. Hilson, *Appl. Radiat. Isot.* 61, 487 (2004).
92. P. Zhang, F.H. Wittmann, T. Zhao, and E.H. Lehmann, *Physica B Condens. Matter* 405, 1866 (2010).
93. A. Kahle, B. Winkler, B. Hennion, and P. Boutrouille, *Rev. Sci. Instrum.* 74, 3717 (2003).
94. L. Josic, A. Steuwer, and E. Lehmann, *Appl. Phys. A Mater. Sci. Process.* 99, 515 (2010).
95. P. Vontobel, E. Lehmann, and W.D. Carlson, *IEEE Trans. Nucl. Sci.* 52, 338 (2005).
96. A.S. Tremsin, J.B. McPhate, J.V. Vallerga, O.H.W. Siegmund, W.B. Feller, E. Lehmann, L.G. Butler, and M. Dawson, *Nucl. Instrum. Methods Phys. Res.* A652, 400 (2011).
97. M. Wilding, C.E. Lesher, and K. Shields, *Nucl. Instrum. Methods Phys. Res.* A542, 290 (2005).
98. G.E. Ice, C.R. Hubbard, B.C. Larson, J.W.L. Pang, J.D. Budal, S. Spooner, and S.C. Vogel, *Nucl. Instrum. Methods Phys. Res.* A539, 312 (2005).
99. J.A. Xu, H.K. Mao, R.J. Hemley, and E. Hines, *Rev. Sci. Instrum.* 75, 1034 (2004).